Joule

Article

Experimental-modeling framework to unveil iridium degradation pathways during intermittent operation in PEMWE

Graphical abstract

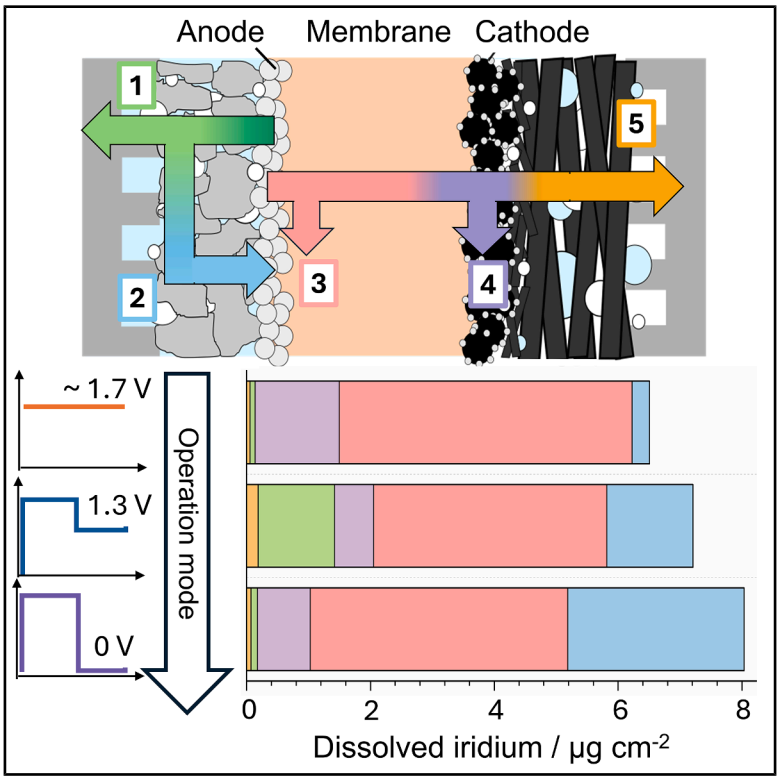

Highlights

- The interplay between Ir dissolution, transport, and deposition processes was disentangled
- The dendritic Ir particles within the membrane promote further encapsulation of Ir ions
- Intermittent operation promotes Ir back-transport to the anode
- Quantitative assessment of Ir stability in MEA was performed

Authors

Maja Milosevic, An Phuc Dam, Mirjam Rogler, ..., Simon Thiele, Kai Sundmacher, Serhiy Cherevko

Correspondence

milosevic@fhi-berlin.mpg.de (M.M.), s.cherevko@fz-juelich.de (S.C.)

In brief

In zero-gap water electrolyzers, deconvoluting anode catalyst degradation pathways is pivotal. Through a combined experimental-modeling approach, we obtained insights into Ir dissolution, transport, and deposition dynamics from a quantitative standpoint. Dissolved Ir species are primarily kept with the membrane electrode assembly through their encapsulation within the Ir band formed at the anode-membrane interface. Intermittent operation further leads to pronounced back-transport of the dissolved species from the water line to the anode, leading to enhanced kinetic losses within an electrolyzer.

Milosevic et al., 2026, Joule *10*, 102309
March 18, 2026
https://doi.org/10.1016/j.joule.2025.102309

CellPress

Joule

CellPress
OPEN ACCESS

Article

Experimental-modeling framework to unveil iridium degradation pathways during intermittent operation in PEMWE

Maja Milosevic,[1,2,6,8,*] An Phuc Dam,[3,4] Mirjam Rogler,[5] Andreas Hutzler,[1] Thomas Böhm,[1] Valentin Briega-Martos,[1,7] Georgios Papakonstantinou,[3] Michel Suermann,[5] Simon Thiele,[1,2] Kai Sundmacher,[4,5] and Serhiy Cherevko[1,*]

[1]Forschungszentrum Jülich GmbH, Helmholtz Institute Erlangen-Nürnberg for Renewable Energy (IET-2), Cauerstr. 1, 91058 Erlangen, Germany
[2]Department of Chemical and Biological Engineering, Friedrich-Alexander University Erlangen, 91058 Erlangen, Germany
[3]Max Planck Institute for Dynamics of Complex Technical Systems, Department Process Systems Engineering, Sandtorstr.1, 39106 Magdeburg, Germany
[4]Department of Process Systems Engineering, Otto-Von-Guericke University Magdeburg, Universitätsplatz 2, 39106 Magdeburg, Germany
[5]Siemens Energy Global GmbH & Co. KG, Freyeslebenstr. 1, 91058 Erlangen, Germany
[6]Present address: Interface Science Department, Fritz-Haber Institute of the Max Planck Society, 14195 Berlin, Germany
[7]Present address: Department of Chemistry and Chemical Biology, Baker Lab, Cornell University, Ithaca, NY 14853, USA
[8]Lead contact
*Correspondence: milosevic@fhi-berlin.mpg.de (M.M.), s.cherevko@fz-juelich.de (S.C.)
https://doi.org/10.1016/j.joule.2025.102309

CONTEXT & SCALE Proton exchange membrane water electrolysis is one of the key technologies within the sustainable energy scenario, combining the intermittent energy delivered by renewable sources with hydrogen production. However, the usage of high amounts of scarce Ir as the anode catalyst is the bottleneck inhibiting the required upscaling of this technology to the terawatt (TW) scale. Reducing Ir loading is necessary, but, in the absence of a good understanding of Ir degradation, it may sacrifice device longevity. With insights into Ir degradation mechanisms primarily limited to those obtained within model systems, the current work addresses this knowledge gap through a combined quantitative and modeling analysis of anode catalyst dissolution within a zero-gap water electrolyzer. Time-dependent tracking of dissolved Ir transport and deposition processes reveals distinct dissolution dynamics dependent on the applied protocols. Furthermore, the developed empirical model demonstrates the impact of Ir back-transport to the anode and Ir band formation on the overall catalyst stability within an electrolyzer, thus creating the groundwork for future reliable analysis of catalyst degradation.

SUMMARY

A deep understanding and mitigation of Ir degradation are crucial for effectively reducing the currently used high catalyst loadings and deploying proton exchange membrane water electrolysis on a gigawatt scale. Here, we deconvolute the dynamics of Ir dissolution, transport, and deposition within an electrolyzer through a combined mass spectrometry-microscopy approach. The formation and consumption of cationic and anionic Ir species are empirically correlated with potential changes during idle periods, while mathematical modeling allows for the quantitative determination of the overall Ir loss. We found that the cationic species precipitate at the anode-membrane interface and, within a short time frame, limit the dissolved ions from accessing the cathode, while potential cycling leads to enhanced back-diffusion of the anionic species to the anode, thus partially entrapping the dissolved Ir. This work suggests that the design of thicker catalyst layers with lower Ir packing densities is an important key to an enhanced durability of electrolyzers.

INTRODUCTION

With the aim of reducing the carbon footprint to combat climate change, renewable energy sources require mitigation methods to cope with their intermittency, with proton exchange membrane water electrolysis (PEMWE) as a promising technology enabling their conversion into green hydrogen through water splitting. The limiting factor is the scarcity of Ir used as the catalyst for the sluggish oxygen evolution reaction (OER) taking place on the anode, as lowering the currently used loadings by at least

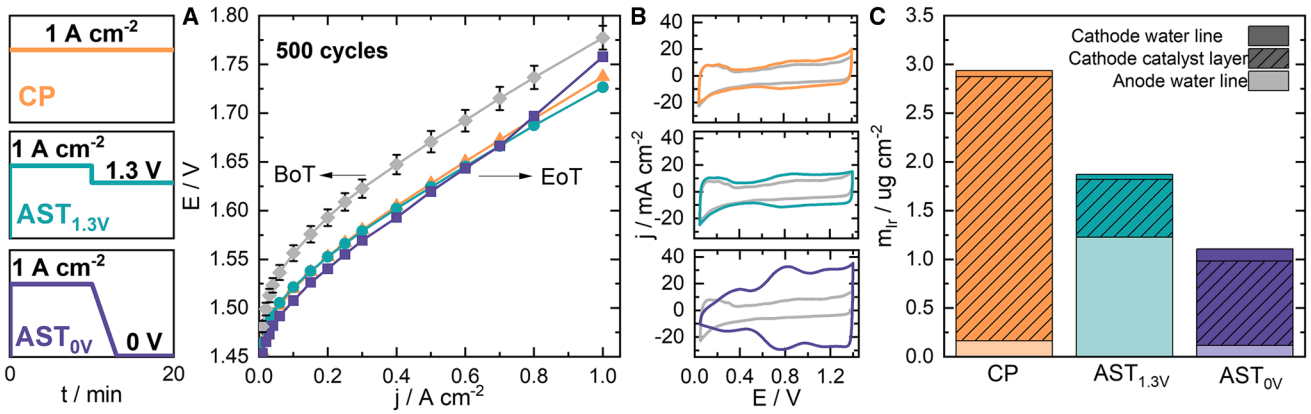

Figure 1. Ambient-pressure PEMWE performance at 60°C recorded during continuous and intermittent operation

(A) Ambient-pressure high frequency resistance (HFR)-free polarization curves recorded after 150 cycles and at the EoT of the 500-cycle CP (orange), $AST_{1.3V}$ (blue), and AST_{0V} (purple).

(B) Cyclic voltammograms of an Ir black anode recorded at the BoT (gray) and at the EoT of the 500-cycle CP (orange), $AST_{1.3V}$ (blue), and AST_{0V} (purple).

(C) ICP-MS-quantified dissolved Ir amounts present in the AWL, CWL, and CCL after 500-cycle CP (orange), $AST_{1.3V}$ (blue), and AST_{0V} (purple), normalized to the surface area of the MEA of 5 cm^2. The error bars represent the standard deviation of three independent measurements.

an order of magnitude is necessary for large-scale deployment of PEMWE.[1–3] To overcome this issue, a deep understanding of Ir degradation mechanisms within an electrolyzer cell is pivotal.

The stability of Ir-based catalysts has been studied extensively over the last couple of decades in aqueous model systems (AMSs)[4–11] due to their simplicity compared with solid electrolytes, where degradation studies are primarily based on electrochemical analysis of cell performance degradation[12–18] and post-mortem characterization of the membrane electrode assemblies (MEAs).[19–21] Within an electrolyzer, catalyst dissolution and its subsequent mass transport have to be studied in parallel due to the balance of migration and diffusion processes between the electrodes exposed to intermittent current loads (herein referred to as electro-diffusion).[22] Although these processes have been shown to significantly influence the movement of cationic contaminants within the MEA layers,[22–24] in AMSs, they are neglected due to the usage of liquid electrolyte, which is the main sink of the dissolved catalyst species. The discrepancy between the two systems with regards to catalyst stability studies has recently been addressed through a quantitative analysis of Ir dissolution within a metal-free electrolyzer. Among the four main Ir sinks, Ir dissolution into the recirculated anode and the cathode water lines (AWL and CWL, respectively) accounted for less than 10% of the total Ir loss, with the majority of the dissolved species shown to deposit either in the membrane adjacent to the anode catalyst layer (ACL), forming the "Ir band," or within the cathode catalyst layer (CCL).[19,20,25] Charge-related absorption tests of Ir dissolution products present in the AWL further showed that although it is primarily the cationic Ir species that are transported through the MEA layers, the anionic species get dissolved into the water phase.[26] Although these studies provide important insights into Ir dissolution and mass transport pathways within an electrolyzer, experimental factors influencing Ir deposition in the CCL and the membrane are poorly understood, especially under intermittent operation. Furthermore, possible changes in the contribution of the cationic and anionic Ir species in the overall Ir loss with time due to the dynamic ACL dissolution processes have not been addressed so far.

In this work, the complexity of Ir dissolution, transport, and deposition within the MEA under various operating conditions is studied through spectrometric-spectroscopic analysis, assisted by mathematical modeling. We quantitatively determine the Ir loss within three dissolved Ir sinks and the contribution of the cationic species to the Ir amount present in the water lines (WLs) using inductively coupled plasma mass spectrometry (ICP-MS).[25,26] The morphology of the Ir band formed at the ACL-membrane interface and the structure of the deposited particles are studied using scanning transmission electron microscopy (STEM) in combination with energy dispersive X-ray spectroscopy (EDXS) mapping. Finally, these results are corroborated with mathematical modeling, through which the influence of Ir transport and deposition processes on the overall measured Ir losses is explained. Taken together, this study elucidates the key role of the electrolysis operation mode in governing not only Ir dissolution but also Ir species transport and redeposition within the system and provides guidelines for future OER catalyst stability studies.

RESULTS AND DISCUSSION

Effect of redox processes on Ir reactivity

Two different accelerated stress tests (ASTs) were performed to analyze the overall electrolyzer performance and Ir black catalyst dissolution under mitigated ($AST_{1.3V}$) and unmitigated (AST_{0V}) intermittent power supply conditions, where within a single AST cycle, a 10-min galvanostatic hold at 1 A cm^{-2} was followed by a 10-min idle potentiostatic period at 1.3 and 0 V, respectively. Steady-state chronopotentiometric (CP) measurements were performed as reference points, with the polarization curves recorded at the beginning of the test (BoT), after 150 AST cycles, and at the end of the test (EoT) of the 500-cycle CP, $AST_{1.3V}$, and AST_{0V} protocols (Figure 1A). It must be noted that the initial drops

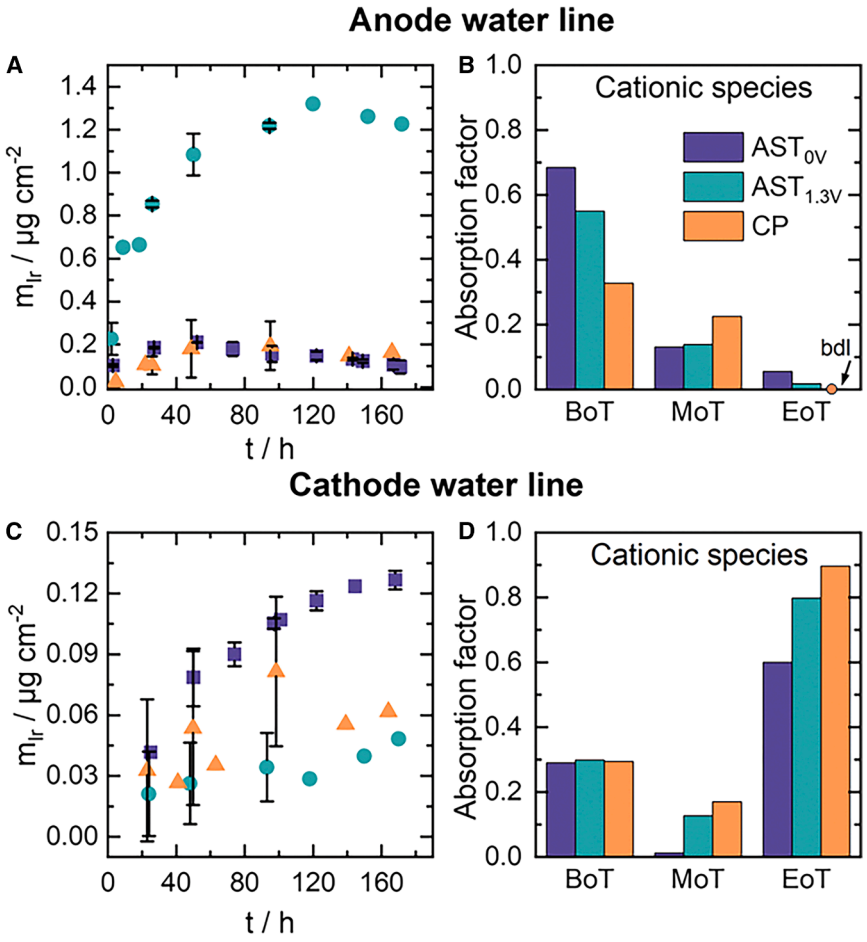

Figure 2. Charge-dependent evolution of Ir dissolution into the water lines under different electrolyzer operation modes

(A and C) Surface-area-normalized total dissolved Ir amount present in the (A) anode and (C) cathode water lines during the 500-cycle CP (orange), $AST_{1.3V}$ (blue), and AST_{0V} (purple), with the averaged values for sampling points from independent measurements taken within the same experimental time window presented with error bars.

(B and D) Absorption factors of the dissolved Ir species present in the (B) anode and (D) cathode water lines at the BoT (10 and 20 h after the beginning of the test, respectively), MoT (after ~96 h), and the EoT of the 500-cycle CP, $AST_{1.3V}$, and AST_{0V} (~170 h). The error bars represent the standard deviation of at least two independent measurements, where sampling was performed within the same time window.

in cell voltage of ~50 mV stem from the break-in phase, which is of a different duration for the three protocols applied, with the ASTs leading to faster voltage stabilization (Figure S1A). As previously reported, the redox processes taking place at the ACL during AST_{0V} lead to the formation of hydrous IrO_x, characteristic of both higher activity and pronounced dissolution at OER conditions.[9,16,25] Although in the initial stages of electrolyzer operation, hydrous IrO_x does lead to an amelioration of cell performance, as shown in Figure S1A,[25,27] prolonged ACL exposure to potential cycling below the reversible cell potential leads to performance degradation by the EoT compared with the $AST_{1.3V}$ and CP protocols. A slight increase in cell voltage is also observed during $AST_{1.3V}$ by the EoT, whereas for steady-state operation, the electrolyzer performance remains stable. The cyclic voltammogram (CV) profiles presented in Figure 1B further reflect the formation of hydrous IrO_x through the appearance of the $Ir^{III/IV}$ redox couple characteristics and the loss of the Ir black-characteristic H-UPD (hydrogen underpotential deposition) features observed at lower potentials, whereas no significant changes in the recorded CVs were observed at the end of $AST_{1.3V}$ and CP, except for a slight loss in OER activity during $AST_{1.3V}$.[8] Although the loss of cell performance during the harsh redox processes within AST_{0V} has previously been attributed to the high Ir dissolution rates, complementary dissolution studies were performed exclusively in AMS.[14,16] Here, the quantification of Ir loss within three different Ir sinks of a single-cell electrolyzer, namely the AWL, CWL, and CCL at the end of the 500-cycle protocols, reveals an inverse dissolution trend compared with that obtained in AMS,[8,9] with the highest amount of dissolved Ir detected during steady-state operation and the lowest for the MEAs exposed to AST_{0V} (Figure 1C). Comparison with our previously reported work reveals that although significant differences in the Ir black dissolution results obtained during AST_{0V} and $AST_{1.3V}$ are shown here, this is not the case for the IrO_x catalyst, where Ir dissolution is ~20 times lower compared with that of Ir black.[25] These observations further attest to the high complexity of the interconnected processes of Ir dissolution, mass transport, and deposition taking place within an electrolyzer, which we discuss in detail in the following sections.

Charge classification of the Ir species

The change in the Ir amount present in the AWL with time, quantified during the 500-cycle protocols, demonstrates that the highest Ir dissolution into the WLs is caused by $AST_{1.3V}$ (Figure 2A), where an initial high Ir dissolution rate is followed by saturation mid-test (MoT) after ~96 h. Although maintaining the potential during idle periods above the reversible cell potential circumvents electrolyzer performance degradation, the ~10 times lower Ir content observed for the CP profile quantitatively demonstrates that continuous potential cycling does lead to a higher Ir dissolution rate in the MEA compared with steady-state operation. As for AST_{0V}, a decline in the Ir amount present in the closed anode water loop occurs after ~60 h, suggesting possible Ir redeposition from the AWL back to the anode during idle periods, which we address in the later discussion.

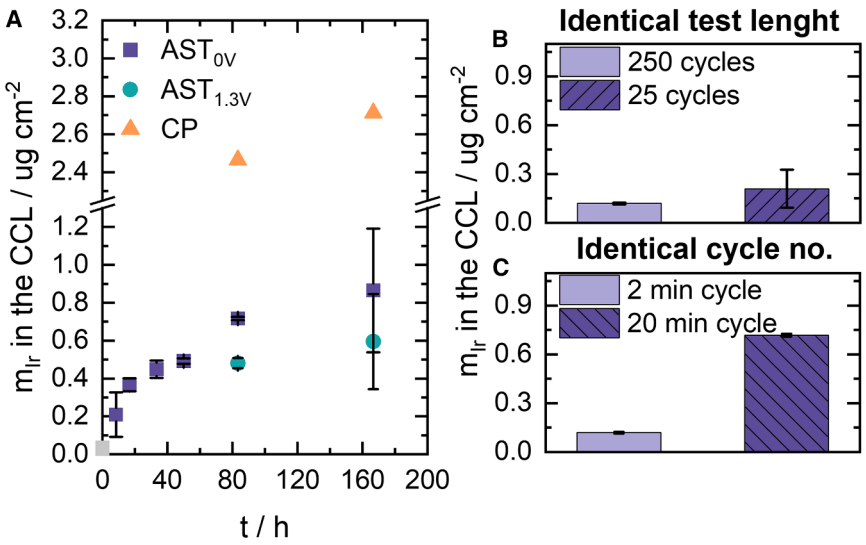

Figure 3. Deposition of the dissolved Ir species within the cathode as a function of time and the protocols applied

(A) The amount of Ir present in the CCL at the EoT under varied experimental time frames (25 to 500 cycles) of AST_{0V} (purple), $AST_{1.3V}$ (blue), and CP (orange), with the Ir amount present in the CCL after the conditioning step serving as a reference (gray square).

(B and C) The influence of (B) the number and (C) the frequency of cycles within AST_{0V} on the Ir amount present in the CCL at the EoT. The error bars represent the standard deviation of at least two independent measurements.

As a further step, time-resolved changes in the contribution of cationic Ir species in both the AWL and the CWL during the 500-cycle AST_{0V}, $AST_{1.3V}$, and CP protocols were tracked to gain additional insights into the Ir dissolution process. The absorption factor, defined as the ratio between the amount of Ir absorbed in the ion exchange material and the initial Ir amount present in the analyzed water sample, was the metric used.[26] Nafion membranes (N117, Ion Power) served as the proton exchange material and, after a conditioning procedure proposed by Dam et al.,[26] were immersed in the analyzed solution for 7 days to ensure complete diffusion of the dissolved Ir ions into the ion exchange membranes. As can be seen in Figure 2B, the species present in the AWL are primarily in the cationic form after ~10 h of testing (BoT samples) for the MEAs exposed to intermittent operation, whereas Ir species dissolved during steady-state operation are predominantly anionic. However, an identical decreasing trend in the contribution of the cationic species with time was observed during all three protocols, with the Ir species present in the AWL being almost completely in the anionic form by the EoT. This observation, together with the pronounced Ir dissolution observed during $AST_{1.3V}$ (Figure 2A), indicates that potential cycling above the reversible cell potential leads to increased dissolution of anionic Ir species.

As for the water that arrives at the cathode side primarily via the electroosmotic drag, the changes in the detected Ir amount with time are almost negligible for all three protocols when compared with the dissolution trends observed in the AWL (Figure 2C), which is in line with our previous reports.[25] And, although the contribution of the Ir present in CWL to the total Ir loss is small, absorption tests complementary to those conducted for the AWL are important for the analysis of Ir transport dynamics in the MEA. The quantified fractions of the cationic species shown in Figure 2D reveal that, in contrast to the results obtained for the AWL, Ir species are mainly in the anionic form after the first ~20 h of operation (BoT sample) and predominantly cationic by the EoT. The obtained absorption results demonstrate that the cationic species do not remain within the AWL but are transported back into the CCM. With knowledge on the mechanism of Ir deposition in the membrane and the CCL being scarce and mostly limited to MEAs exposed to steady-state operation,[20,25] information on Ir deposition as a function of both time and the protocols applied is essential for studies focused on Ir degradation in PEMWE.

Ir dissolution and transport toward the CCL

With the AST_{0V} protocol leading to a significant degradation in electrolyzer performance compared with the mitigated intermittent ($AST_{1.3V}$) and steady-state (CP) operation (Figure 1A), the influence of time on the Ir amount present in the CCL was evaluated through post-mortem quantitative analysis of MEAs exposed to an increasing number of AST_{0V} cycles (25 to 500 cycles) via a chemical digestive procedure reported in our previous work.[25] As can be observed in Figure 3A, the electro-diffusion-induced Ir transport toward the cathode is most pronounced within the first 40 h of electrochemical testing, with Ir transport toward the cathode slowing down after ~80 h (250 cycles) and ultimately stabilizing after ~160 h (500 cycles). With the purpose of discovering to what extent circumventing the redox electrochemistry of Ir during AST_{0V} leads to a change in the observed trend in Ir dissolution and transport, post-mortem analysis of MEAs exposed to 250- and 500-cycle $AST_{1.3V}$ and CP was also performed. Although it is observed that the influence of electro-diffusion processes leads to the same stabilization trend for all three protocols, the formation of hydrous IrO_x during AST_{0V} does not lead to significantly higher Ir transport toward the CCL compared with the other protocols. On the contrary, the Ir amount present in the CCL at the end of CP tests significantly supersedes that obtained during both ASTs, which is contrary to numerous works on Ir degradation that attribute the increase in the Ir dissolution rate to operational intermittency, which will be addressed in the subsequent sections.[8,9,13,16,28,29]

With previous reports showing that an increase in the cycling speed within an AST leads to a severe decrease in OER kinetics,[15] a 10-times-faster 250-cycle AST_{0V} (2 min per cycle) was performed for further analysis of Ir transport. Surprisingly, Ir transport and deposition at the CCL are shown to be independent of the cycling frequency, as comparable Ir amounts were

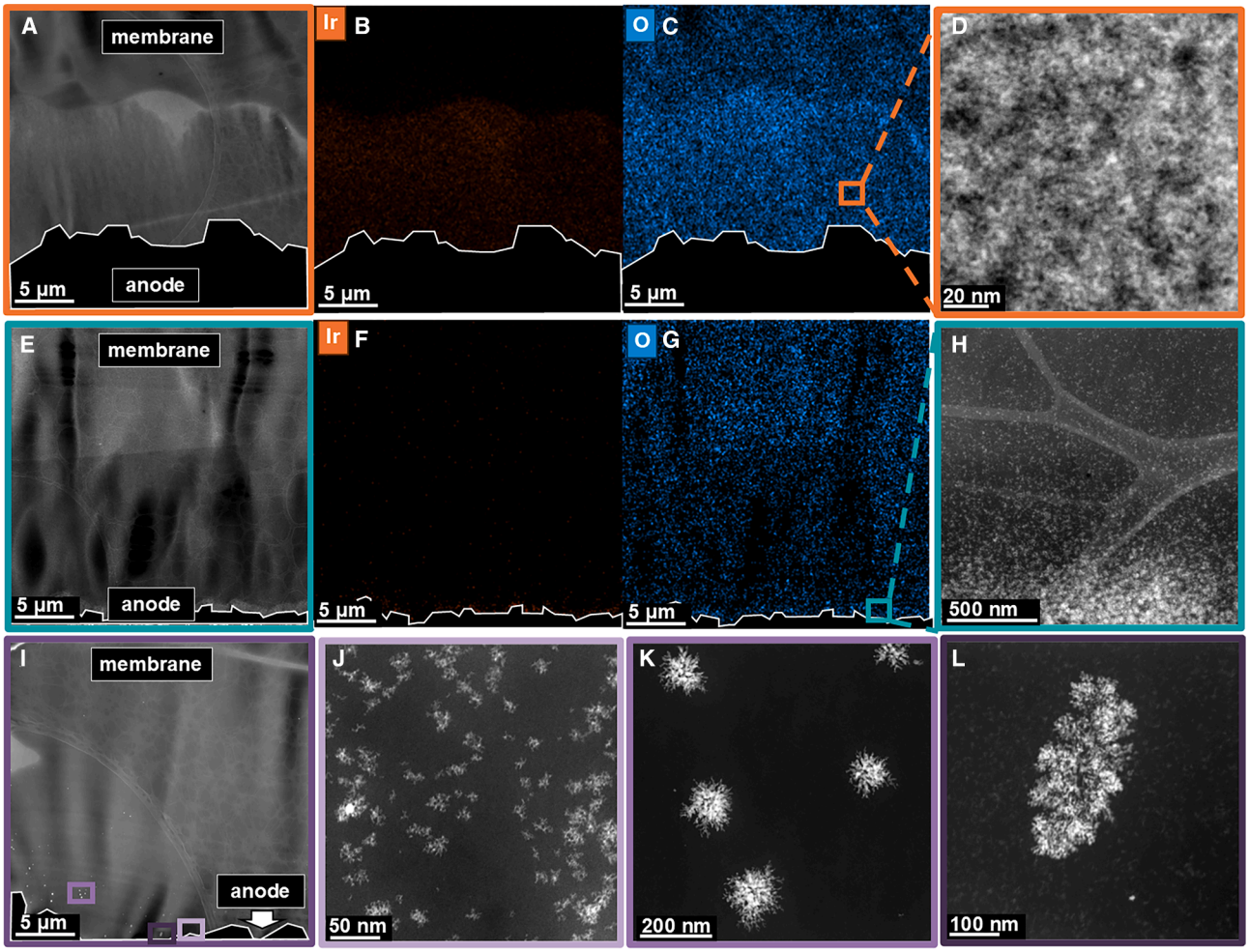

Figure 4. Ir band morphology variations following continuous and intermittent electrolyzer operation

HAADF-STEM micrographs of the ACL-membrane interface with the corresponding EDXS results for the MEAs exposed to 500-cycle (A)–(D) CP (orange), (E)–(H) $AST_{1.3V}$ (blue), and (I)–(L) AST_{0V} (purple).

quantified in the cathode for both the standard and the faster AST_{0V} protocol of equal duration (Figure 3B). Comparison between the two experiments of equal cycle number (250 cycles) further demonstrates the influence of the total cycling time on Ir transport, with the long cycle leading to ~4 times higher Ir deposition in the cathode (Figure 3C).

The results presented in this section are contrary to those observed in AMS[8,9,25,28] and can be attributed to the following factors, which will be further elaborated: (1) redeposition of the dissolved Ir species close to the ACL-membrane interface,[19,20] (2) Ir diffusion during idle periods within the performed ASTs, and (3) redeposition of Ir ions from the AWL to the ACL.

Dissolution-driven morphological changes at the ACL-membrane interface

High-angle annular dark-field (HAADF)-STEM images of MEA cross-sections exposed for ~170 h to the three protocols show apparent differences in the "Ir band" morphology (Figure 4). When the electrolyzer is operated under steady state (Figure 4B) and mitigated intermittent conditions (Figure 4C), distinctive oxide-based "Ir bands" are formed (Figure S2), with thicknesses of ~10 and ~1 μm, respectively. However, during AST_{0V}, inhomogeneously distributed Ir particles are observed up to 20 μm into the membrane (Figure 4D). Lowering of the potential during idle periods is shown to lead to the formation of larger Ir particles with distinct dendritic features (Figure S3), indicating a higher Ir dissolution rate under intermittent operation, especially during the harsher AST_{0V}, where the segregation of the dissolved Ir species takes precedence over the formation of a homogeneous "Ir band." The loss of these features further into the membrane (Figure S4) further suggests that the dynamic Ir dissolution-deposition process within the Ir band during AST_{0V} primarily occurs in proximity to the anode. A potential-dependent growth of different nanostructures via dissolution-redeposition processes was reported for Cu during the CO_2 reduction reaction,[30] and a similar effect involving dissolution and precipitation of Pt within the membrane in the form of a "Pt band" due to the reaction with crossover H_2 was observed for PEM

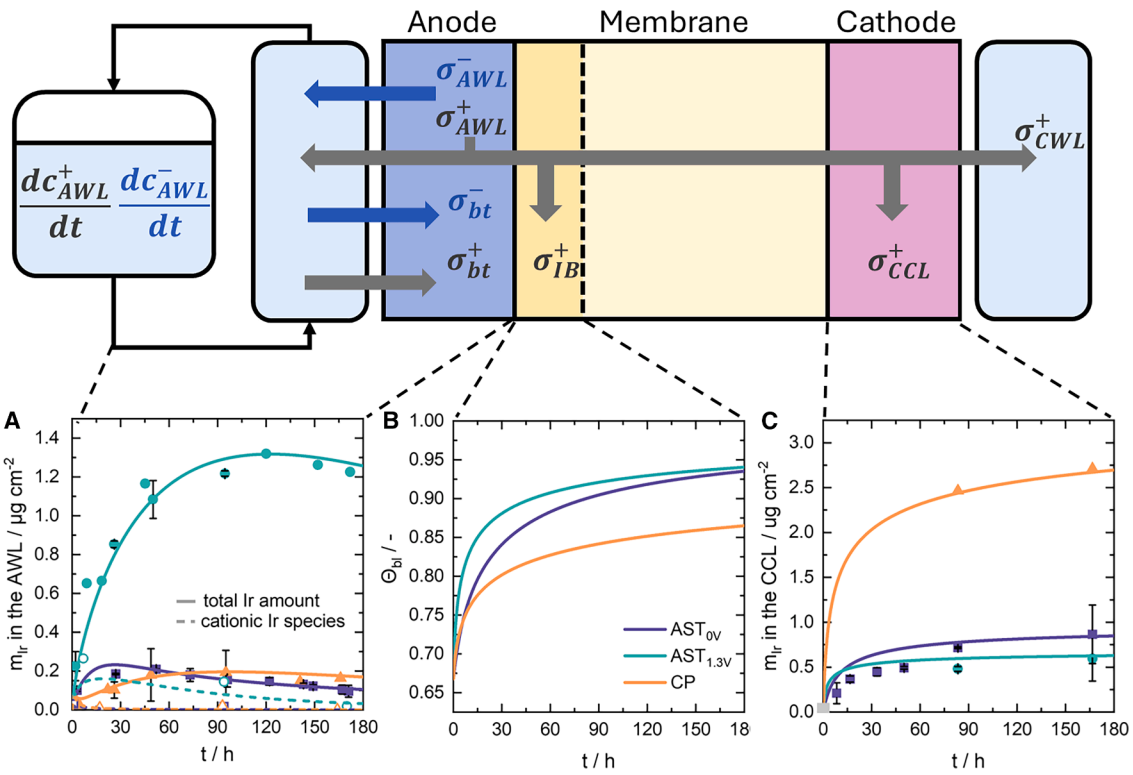

Figure 5. The empirical model deconvoluting charge-dependent Ir degradation pathways at different MEA operating conditions

Schematic of the developed quasi-stationary 0D model with the indicated source and sink terms for Ir ions.

(A–C) Ir amount present in the anode water line, (B) probability of Ir depositing at the ACL-membrane interface, and (C) Ir amount deposited in the cathode. The experimental results are presented by full symbols and the model simulations by solid lines, with the hollow symbols and the dashed lines in (A) showing the quantified and modeled contribution of the Ir^{3+} species in AWL, respectively.

fuel cells.[31] Moreover, both the position of the "Pt band" and the local membrane potential at the catalyst-membrane interfaces were shown to depend on the H_2/O_2 partial pressure ratio.[32,33] Taking into consideration that the H_2 concentration at the ACL-membrane interface is more pronounced during intermittent operation[33,34] when the pronounced formation of the dendritic Ir particles was observed (Figures 4H and 4L), low Ir crossover toward the cathode during AST_{0V} and $AST_{1.3V}$ can be explained.

Inter-relations between Ir dissolution, transport, and deposition and modeling insights

To support the obtained dissolution and microscopy results and address the influence of Ir transport and deposition on the overall Ir losses, a mathematical model was developed. Foremost, it must be pointed out that the overall charge of the dissolved species has a crucial influence on their further transport within an electrolyzer system and must be considered during model formation. The performed absorption tests revealed that the cationic species are transported toward the CWL (Figures 2B and 2D), forming the Ir band (Figure 4) and depositing in the cathode (Figure 3) along the way, while the dissolved anionic species are primarily transported into the anode water loop (Figure 2B).[35] With speciation of the anionic and cationic Ir species challenging, in the following discussion, IrO_4^{2-} and Ir^{3+} will be considered as the main Ir dissolution products based on thermodynamics (Figure S5) and the reported works on Ir dissolution mechanisms in aqueous electrolyte,[8,11] discussed in detail in the Note S1. Initial investigation on the dynamics of transport and deposition of Ir^{3+} within the cathode through a 1D dynamic transport model (Scheme S1) demonstrates that Ir deposition in the CCL is a fast process, as slow deposition would lead to the formation of the Ir band adjacent to the CCL (Figure S6), not the ACL as found here (Figures 4 and S2–S4). Furthermore, the simulations show that the fraction diffusing from the membrane domain back to the anode region during the idle phases increases with cycle frequency (Figure S7), which elaborates on the observed decrease in the amount of Ir present in the CCL when decreasing the cycle length by 10-fold (Figure 3B). For long cycle times of 20 min primarily used in this work, the back-diffusion becomes negligible. Consequently, it is a good approximation to use a simplified quasi-stationary 0D model approach, neglecting the effect of dynamic operation on ion transport.

The general scheme of the 0D model is shown in Figure 5. The performed simulations are in good correlation with the experimental results (Figures 5A–5C), with the model suggesting that back-transport of Ir ions from the AWL back to the anode occurs during all three protocols, though to a significantly greater extent

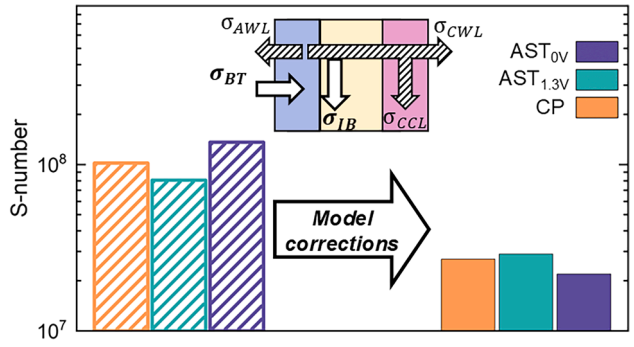

Figure 6. The impact of the proposed experimental-modeling framework on Ir stability determination in MEA

Comparison of Ir black stability after the 500-cycle AST$_{0V}$, AST$_{1.3V}$, and CP expressed through the S-number metric. S-numbers obtained by considering only the Ir sinks quantifiable via ICP-MS (the water lines and the cathode) are presented with patterned bars, whereas the S-numbers derived by also accounting for the influence of the model-obtained Ir back-diffusion and Ir band formation are presented as full bars.

during intermittent operation (Figure S8). The concentration in the AWL becomes constant during the AST$_{1.3V}$ protocol when the Ir dissolution rate approximately equals the rate of Ir redeposition into the ACL, with ~50% of the total Ir amount in the AWL being transported back to the anode during 180 h of operation. Furthermore, the absorption tests revealed that the higher Ir dissolution flow into the AWL during AST$_{1.3V}$ compared with CP is due to the increased formation of IrO_4^{2-}. Although in AMS it was reported that longer exposure of the anode to the OER potentials leads to higher IrO_4^{2-} formation, pronounced IrO_4^{2-} presence in the AWL during potential cycling above the reversible cell potential can be attributed to the potential spikes at the anode during protocol transition periods, as suggested in the literature.[13] The pronounced Ir dissolution as a result of intermittent operation is also expected to take place during AST$_{0V}$, with the model simulations suggesting that the observed decrease in the Ir content in the AWL is the result of enhanced redeposition of Ir species into the ACL. These observations suggest that entrapment of the Ir dissolved within the active anode zone due to the oscillations in the applied current loads can be promoted by utilizing thicker ACLs. To synchronize this process with the increasing necessity for lower Ir loadings, the development of novel Ir-based catalysts with lower Ir packing densities is pivotal for creating longer transportation pathways for the dissolved Ir within low-loading MEAs.

As for the formation of the Ir band under different protocols, an empirical sigmoidal correlation was implemented to describe the expected behavior of the Ir band, with the blockage probability of Ir^{3+} ions (Θ_{bl}) expressed as a function of the amount of Ir already deposited in the Ir band, n_{ib} *[mol]*:

$$\Theta_{bl} = \Theta_{bl,pt} + \left(1 - \Theta_{bl,pt}\right) \frac{1}{1+exp\left(-a\left(n_{ib} - b\right)\right)}$$

$\Theta_{bl,pt}$ *[-]* presents the probability of Ir ions being deposited prior to the formation of the Ir band, *b [mol]* corresponds to the Ir amount present when 50% of the transition of the sigmoidal function occurs, and *a [mol^{-1}]* describes the steepness of the transition. The model reveals that the probability of migrating Ir^{3+} being blocked and deposited (Θ_{bl}) increases as the band grows, especially during dynamic electrolyzer operation (Figure 5B), which can be related to the formation of the IrO_2 dendritic structures within the band and the higher H_2 in O_2 concentration present at the ACL-membrane interface during idle periods, as discussed in the Note S2. Furthermore, the simulations indicate that, already after ~100 h of operation, only a small fraction of the migrating Ir can pass through the Ir band toward the cathode (Figures 5B, 5C, and S9), leading to the Ir band becoming a major sink for the dissolved Ir species. Details on the development of the models used can be found in the Notes S3 and S4. It must be noted that, in this work, the model-based analysis focused on the standard 20-min cycle time. For modeling higher frequencies of the intermittent operation, a 1D modeling approach would be preferable to achieve higher simulation accuracy.

The modeling simulations further contributed to the catalyst stability assessment in MEA. If we were to express the Ir black stability through the S-number metric[10] by considering exclusively the quantifiable Ir losses, the anode exposed to the AST$_{0V}$ would be the most stable after ~180 h of operation. However, incorporation of the model-derived contributions of back-transport and Ir band formation leads to not only a slight decrease in the obtained S-numbers but also a partially inverted trend between the three tested protocols, with the Ir black anode exposed to AST$_{0V}$ exhibiting the lowest S-number (Figures 6 and S10). Further long-term MEA tests addressing the continuous formation of a homogeneous Ir band during AST$_{1.3V}$ and ACL restructuring caused by redox processes during AST$_{0V}$ are pivotal for the formation of a quantifiable correlation between the Ir degradation mechanisms presented here and their evolution over longer operational periods. Although such a testing campaign is outside the scope of this work, the observations reported here allow for the formation of a multi-step evaluation strategy, described in detail in Note S5, which should be used for future reliable analysis of catalyst stability.

Conclusions

The combined ICP-MS, STEM-EDXS, and modeling approach presented in this work unravels the influence of the operating conditions on Ir degradation pathways within a PEM water electrolyzer. Although Ir dissolution has been suggested as the main culprit behind performance degradation under intermittent operation, quantitative analysis of Ir loss, corroborated by the empirical model presented here, unravels the dynamic evolution of Ir dissolution, transport, and deposition processes that simultaneously take place within an electrolyzer, demonstrating the following:

(1) the crucial role of reductive potentials during idle periods on enhanced Ir redeposition to the ACL, with the process even masking the dissolution of anionic IrO_4^{2-} species into the WL;
(2) the obstruction of the migrating Ir ions due to the formation of the Ir band after ~50 h of operation, with the probability of Ir precipitation being higher during idle phases of intermittent operation through the formation of Ir particles with dendritic features; and

(3) the possibility of using the OER catalyst content in the cathode for initial catalyst stability evaluation of novel materials on a single-cell level when short-term tests are performed.

We believe that the most crucial aspect of the analysis approach presented is a significant reduction in uncertainties inherent to Ir degradation studies reported so far. The insights provided allow for the formation of good practices in future OER catalyst stability studies. Furthermore, they unveil the necessity of developing novel Ir-based materials with lower packing densities to promote the encapsulation of the Ir species dissolved during intermittent operation within the active OER zone. Our work presents an essential step toward knowledge-based mitigation strategies for optimizing state-of-the-art PEM electrolyzers and decreasing the high Ir loadings currently used. Beyond PEMWE, this study prepares the ground for future research directives focused on understanding the dynamics of relevant material changes within multiple zero-gap electrochemical systems.

METHODS

MEA specifications

An in-house-designed model electrolyzer cell with an active area of 5 cm^2 was used in this work. The MEAs consisted of a perfluorosulfonic acid (PFSA)-based membrane, a Pt black hydrogen cathode, and an Ir black oxygen anode, with the loadings of 0.6 mg_{Pt} cm^{-2} and 1.2 mg_{Ir} cm^{-2}, respectively. Carbon felt fiber paper (H24 C5-A4 from Freudenberg, with a microporous layer [MPL]), with a thickness of 280 ± 10 μm, and sintered titanium (Mott Corporation, USA), with a porosity of ∼50% and a thickness of 280 ± 10 μm, were used as porous transport layers (PTLs) at the cathode and anode, respectively.

Electrochemical characterization

MEAs were tested in a metal-free PEMWE test station at 60°C, at atmospheric pressure, with de-ionized (DI) water being supplied only to the anode side of the electrolyzer, through a closed water loop, at a flow rate of 5 mL min^{-1}, as described in our previous work.[25] Initially, the electrolyzer cell was conditioned at 1 A cm^{-2} for 1 h, followed by an electrochemical characterization of the MEA that was used as a reference point for all subsequent measurements, consisting of 3 CVs recorded in the potential range of 0.05–1.4 V at a scan rate of 50 mV s^{-1} and a polarization curve measured by increasing the current density from 0.01 to 1 A cm^{-2} stepwise, holding each current for 2 min to ensure stable cell voltage. Additionally, AC impedance measurements were performed at the end of each current density step in a frequency range of 100 kH to 100 mHz, with the amplitude of the current perturbation being maintained always <20% of the applied current. The high-frequency intercept with the real axis in the Nyquist plot was used to determine the high-frequency resistance of the cell.

Degradation test protocols

A variety of factors influencing ACL dissolution were evaluated in this work, including the protocol type (continuous and intermittent operation), stressor severity (cell voltage during idle periods within the performed ASTs), and experimental duration. During $AST_{1.3V}$, the cell voltage was kept at 1.3 V for 10 min after the 10-min galvanostatic hold at 1 A cm^{-2}, whereas during AST_{0V} the 10-min chronopotentiometric hold at 1 A cm^{-2} was followed by linear sweep voltammetry (LSV) from 1.7 to 0 V at a scan rate of 10 mV s^{-1} and a subsequent potentiostatic hold at 0 V, altogether creating an idle period step of 10 min. Steady-state operation measurements were also performed as reference points. For the sake of easier comparison with the ASTs used in this work, a 20-min cycle of the steady-state chronopotentiometric operation at 1 A cm^{-2} was used as a metric to describe the length of the CP protocols performed. Electrochemical cell characterization via CV, impedance measurements, and recording of polarization curves was performed after 50 cycles of each individual measurement.

Quantification of Ir dissolution

The quantification of catalyst species dissolved in the WLs was performed *ex situ* using an ICP-MS (Perkin – Elmer, NexION 350). The anode and cathode water samples were taken periodically during the course of all performed measurements, as well as at the end of the 1-h conditioning phase. To quantify the amount of Ir present in the CCL, the cathode was chemically digested in aqua regia and afterward analyzed as a bulk solution with ICP-MS. At least 2 post-mortem digestive analyses of the Ir content in the CCL were performed for all the measurements to ensure the reproducibility of the results. An internal standard of 10 $\mu g \cdot L^{-1}$ of Re (Merck Centripur) in 1 wt.% HNO_3 (Suprapur, Merck) was used, and a four-point calibration was carried out with a blank and three standard Ir solutions (0, 0.5, 1, 5 $\mu g_{Ir} \cdot L^{-1}$) every day before performing the measurements presented in this work. Details on the quantification of Ir dissolution in MEA have been provided in a previous publication from our group.[25]

Testing the charge of Ir dissolution products

After the completion of various electrochemical tests described above (namely 500-cycle AST_{0V}, 500-cycle $AST_{1.3V}$, and 500-cycle CP), absorption tests of the anode and cathode water samples were performed. Nafion membranes (N117, Ion Power) were used as a proton exchange material and pretreated at 80°C in 5% H_2O_2, 1 M H_2SO_4, and DI water for 2 h at a time before the start of the absorption tests. The volume of the water sample and the membrane size used for each separate absorption test were 25 mL and 5 cm^2, respectively, with the membrane being immersed in the analyzed solution for 7 days to ensure complete diffusion of the dissolved Ir ions into the ion exchange membranes. The Ir content was quantified via ICP-MS before the membrane immersion and immediately after the end of the absorption tests. Changes in the charge of the Ir species with time were probed by analyzing three samples taken at different time frames: (1) BoT samples taken from the anode and cathode WLs 10 and 20 h after the start of the experiment, respectively; (2) MoT samples taken from the WLs after 4 days; and (3) EoT samples taken after the end of the electrochemical tests. Additional details on the absorption tests procedure are provided elsewhere by Dam et al.[26]

Structural analysis of the ACL-membrane interface

STEM was used for structural analysis of the Ir bands in the membrane in close proximity to the ACL. The Talos F200i (Thermo Fisher Scientific) was equipped with a Schottky field-emission gun (X-FEG) and a Dual Bruker XFlash 6 | 100 EDXS detector. Imaging was carried out at a primary electron energy of 200 keV, a beam current of 40 pA, and a convergence angle of 10.5 mrad. A HAADF detector allowed detection of elastically scattered electrons in an angle range between 58 and 200 mrad. STEM-EDXS was performed to determine the composition of the Ir particles present at the ACL-membrane interface. The MEA samples were prepared by ultramicrotomy. After electrochemical measurements, the MEAs were embedded in Araldite 502 epoxy resin and cut on an RMC Boeckeler PowerTome using a Diatome ultra 45° diamond knife. The sections were collected afterward on lacey carbon-coated copper grids.

Modeling

Two different types of models are developed and analyzed in this work: a 1D and a 0D dynamic model. The 1D model is developed based on the Nernst-Planck equation and Ohm's law to study the influence of the dynamic diffusion of Ir cations during the idle phases back to the ACL, whereas a simplified dynamic 0D quasi-stationary modeling approach is proposed to mathematically describe the experimental data. The AWL is considered as ideally mixed, as the strong bubbling in the cell and the convective flow due to the pumping in recirculation reduce the Ir concentration gradients in the water phase, with the Ir cations being (re-)absorbed into the ionomer phase of the ACL and the anionic Ir redepositing on the surface of catalyst particles in the ACL. The transport of both the Ir cations and anions from the AWL back into the ACL is modeled using first-order reaction kinetics with respect to the concentration of the dissolved species in the AWL. As for the Ir ion transport directions, they are approximated in accordance with previous reports showing that 93% of Ir cations migrate toward the cathode and that Ir anions are fully transported into the AWL, from where they can deposit back into the ACL.[26] A reciprocal dependence of the dissolution rate on the OER operation time is considered, as has been found in a previous work[33] (S 21), while the probability of Ir cations migrating to the cathode to be blocked and deposited in the Ir band is empirically described by a sigmoidal function (S 23). For the ASTs, a quasi-stationary simplification is used in which the intermittent operation is treated as if it were stationary and the different response of the system in terms of dissolution, transport, and deposition of Ir ions is accounted for by estimating apparent model parameters that average the effect of the on and idle phases. Consequently, identical model equations are considered for CP and ASTs. Further details of the model development are given in Notes S3 and S4.

RESOURCE AVAILABILITY

Lead contact

Requests for further information and resources should be directed to, and will be fulfilled by, the lead contact, Maja Milosevic (milosevic@fhi-berlin.mpg.de).

Materials availability

This study did not generate new unique reagents.

Data and code availability

The source data files for Figures 1–3, 5, and 6, and the modeling work generated within the present study, are available within the GitHub depository at https://github.com/APD-git/QS-model-PEMWE-Ir-dissolution.git and https://github.com/APD-git/1D-model-for-dynamic-tranpsort-of-Ir-in-the-CCM.git.

ACKNOWLEDGMENTS

The authors would like to acknowledge Siemens Energy for financial support within the research contract "PEMWE age." The EU program ERDF (European Regional Development Fund) of the German Federal State Saxony-Anhalt within the Research Center of Dynamic Systems (CDS) and the MaxNet Energy research consortium of the Max Planck Society are gratefully acknowledged for financial support. This work is also part of the research initiative "SmartProSys: Intelligent Process Systems for the Sustainable Production of Chemicals," funded by the Ministry for Science, Energy, Climate Protection and the Environment of the State of Saxony-Anhalt.

AUTHOR CONTRIBUTIONS

M.M. and S.C. conceived and planned the experiments. M.M. carried out the electrochemical and dissolution measurements. M.R. prepared the MEA samples. A.P.D. developed the 1D dynamic and 0D quasi-stationary models and processed the corresponding data. T.B. prepared the MEA samples for TEM imaging and A.H. conducted structural analysis using STEM. M.M. analyzed and summarized the experimental data. V.B.-M., G.P., M.S., S.T., K.S., and S.C. contributed to the interpretation of the results. M.M. took the lead in writing the manuscript. All the authors provided critical feedback and helped shape the research, analysis, and manuscript.

DECLARATION OF INTERESTS

The authors declare no competing interests.

SUPPLEMENTAL INFORMATION

Supplemental information can be found online at https://doi.org/10.1016/j.joule.2025.102309.

Received: February 3, 2025
Revised: April 11, 2025
Accepted: December 23, 2025
Published: March 2, 2026

REFERENCES

1. Minke, C., Suermann, M., Bensmann, B., and Hanke-Rauschenbach, R. (2021). Is iridium demand a potential bottleneck in the realization of large-scale PEM water electrolysis? Int. J. Hydrog. Energ. *46*, 23581–23590. https://doi.org/10.1016/j.ijhydene.2021.04.174.
2. Hubert, M.A., King, L.A., and Jaramillo, T.F. (2022). Evaluating the Case for Reduced Precious Metal Catalysts in Proton Exchange Membrane Electrolyzers. ACS Energy Lett. *7*, 17–23. https://doi.org/10.1021/acsenergylett.1c01869.
3. Clapp, M., Zalitis, C.M., and Ryan, M. (2023). Perspectives on current and future iridium demand and iridium oxide catalysts for PEM water electrolysis. Catal. Today *420*, 114140. https://doi.org/10.1016/j.cattod.2023.114140.
4. Reier, T., Nong, H.N., Teschner, D., Schlögl, R., and Strasser, P. (2017). Electrocatalytic Oxygen Evolution Reaction in Acidic Environments - Reaction Mechanisms and Catalysts. Adv. Energy Mater. *7*. https://doi.org/10.1002/aenm.201601275.
5. Reier, T., Oezaslan, M., and Strasser, P. (2012). Electrocatalytic Oxygen Evolution Reaction (OER) on Ru, Ir, and Pt Catalysts: A Comparative Study

of Nanoparticles and Bulk Materials. ACS Catal. *2*, 1765–1772. https://doi.org/10.1021/cs3003098.

6. Spöri, C., Kwan, J.T.H., Bonakdarpour, A., Wilkinson, D.P., and Strasser, P. (2017). The Stability Challenges of Oxygen Evolving Catalysts: Towards a Common Fundamental Understanding and Mitigation of Catalyst Degradation. Angew. Chem. Int. Ed. *56*, 5994–6021. https://doi.org/10.1002/anie.201608601.
7. Cherevko, S., Geiger, S., Kasian, O., Kulyk, N., Grote, J.P., Savan, A., Shrestha, B.R., Merzlikin, S., Breitbach, B., Ludwig, A., et al. (2016). Oxygen and hydrogen evolution reactions on Ru, RuO_2, Ir, and IrO2 thin film electrodes in acidic and alkaline electrolytes: A comparative study on activity and stability. Catal. Today *262*, 170–180. https://doi.org/10.1016/j.cattod.2015.08.014.
8. Cherevko, S., Geiger, S., Kasian, O., Mingers, A., and Mayrhofer, K.J.J. (2016). Oxygen evolution activity and stability of iridium in acidic media. Part 1. - Metallic iridium. J. Electroanal. Chem. *773*, 69–78. https://doi.org/10.1016/j.jelechem.2016.04.033.
9. Cherevko, S., Geiger, S., Kasian, O., Mingers, A., and Mayrhofer, K.J.J. (2016). Oxygen evolution activity and stability of iridium in acidic media. Part 2. - Electrochemically grown hydrous iridium oxide. J. Electroanal. Chem. *774*, 102–110. https://doi.org/10.1016/j.jelechem.2016.05.015.
10. Geiger, S., Kasian, O., Ledendecker, M., Pizzutilo, E., Mingers, A.M., Fu, W.T., Diaz-Morales, O., Li, Z.Z., Oellers, T., Fruchter, L., et al. (2018). The stability number as a metric for electrocatalyst stability benchmarking. Nat. Catal. *1*, 508–515. https://doi.org/10.1038/s41929-018-0085-6.
11. Kasian, O., Grote, J.P., Geiger, S., Cherevko, S., and Mayrhofer, K.J.J. (2018). The Common Intermediates of Oxygen Evolution and Dissolution Reactions during Water Electrolysis on Iridium. Angew. Chem. Int. Ed. *57*, 2488–2491. https://doi.org/10.1002/anie.201709652.
12. Alia, S.M., Reeves, K.S., Cullen, D.A., Yu, H.R., Kropf, A.J., Kariuki, N., Park, J.H., and Myers, D.J. (2024). Simulated Start-Stop and the Impact of Catalyst Layer Redox on Degradation and Performance Loss in Low-Temperature Electrolysis. J. Electrochem. Soc. *171*, 044503. https://doi.org/10.1149/1945-7111/ad2bea.
13. Alia, S.M., Reeves, K.S., Yu, H.R., Park, J., Kariuki, N., Kropf, A.J., Myers, D.J., and Cullen, D.A. (2022). Electrolyzer Performance Loss from Accelerated Stress Tests and Corresponding Changes to Catalyst Layers and Interfaces. J. Electrochem. Soc. *169*, 054517. https://doi.org/10.1149/1945-7111/ac697e.
14. Alia, S.M., Reeves, K.S., Yu, H.R., Park, J.H., Kariuki, N.N., Kropf, A.J., Myers, D.J., and Cullen, D.A. (2024). Catalyst-Specific Accelerated Stress Tests in Proton Exchange Membrane Low-Temperature Electrolysis for Intermittent Operation. J. Electrochem. Soc. *171*, 024505. https://doi.org/10.1149/1945-7111/ad2735.
15. Alia, S.M., Stariha, S., and Borup, R.L. (2019). Electrolyzer Durability at Low Catalyst Loading and with Dynamic Operation. J. Electrochem. Soc. *166*, F1164–F1172. https://doi.org/10.1149/2.0231915jes.
16. Weiß, A., Siebel, A., Bernt, M., Shen, T.H., Tileli, V., and Gasteiger, H.A. (2019). Impact of Intermittent Operation on Lifetime and Performance of a PEM Water Electrolyzer. J. Electrochem. Soc. *166*, F487–F497. https://doi.org/10.1149/2.0421908jes.
17. Möckl, M., Ernst, M.F., Kornherr, M., Allebrod, F., Bernt, M., Byrknes, J., Eickes, C., Gebauer, C., Moskovtseva, A., and Gasteiger, H.A. (2022). Durability Testing of Low-Iridium PEM Water Electrolysis Membrane Electrode Assemblies. J. Electrochem. Soc. *169*, 064505. https://doi.org/10.1149/1945-7111/ac6d14.
18. Lettenmeier, P., Wang, R., Abouatallah, R., Helmly, S., Morawietz, T., Hiesgen, R., Kolb, S., Burggraf, F., Kallo, J., Gago, A.S., et al. (2016). Durable Membrane Electrode Assemblies for Proton Exchange Membrane Electrolyzer Systems Operating at High Current Densities. Electrochim. Acta *210*, 502–511. https://doi.org/10.1016/j.electacta.2016.04.164.
19. Yu, H.R., Bonville, L., Jankovic, J., and Maric, R. (2020). Microscopic insights on the degradation of a PEM water electrolyzer with ultra-low catalyst loading. Appl. Catal. B *260*, 118194. https://doi.org/10.1016/j.apcatb.2019.118194.
20. Zeng, Z., Ouimet, R., Bonville, L., Niedzwiecki, A., Capuano, C., Ayers, K., Soleymani, A.P., Jankovic, J., Yu, H., Mirshekari, G., et al. (2022). Degradation Mechanisms in Advanced MEAs for PEM Water Electrolyzers Fabricated by Reactive Spray Deposition Technology. J. Electrochem. Soc. *169*, 054536. https://doi.org/10.1149/1945-7111/ac7170.
21. Zaccarine, S.F., Shviro, M., Weker, J.N., Dzara, M.J., Foster, J., Carmo, M., and Pylypenko, S. (2022). Multi-Scale Multi-Technique Characterization Approach for Analysis of PEM Electrolyzer Catalyst Layer Degradation. J. Electrochem. Soc. *169*, 064502. https://doi.org/10.1149/1945-7111/ac7258.
22. Zlobinski, M., Babic, U., Fikry, M., Gubler, L., Schmidt, T.J., and Boillat, P. (2020). Dynamic Neutron Imaging and Modeling of Cationic Impurities in Polymer Electrolyte Water Electrolyzer. J. Electrochem. Soc. *167*, 144509. https://doi.org/10.1149/1945-7111/abc83b.
23. Babic, U., Zlobinski, M., Schmidt, T.J., Boillat, P., and Gubler, L. (2019). CO2-Assisted Regeneration of a Polymer Electrolyte Water Electrolyzer Contaminated with Metal Ion Impurities. J. Electrochem. Soc. *166*, F610–F619. https://doi.org/10.1149/2.0851910jes.
24. Joensen, B.Ó., Zamora Zeledón, J.A., Trotochaud, L., Sartori, A., Mirolo, M., Moss, A.B., Garg, S., Chorkendorff, I., Drnec, J., Seger, B., et al. (2024). Unveiling transport mechanisms of cesium and water in operando zero-gap CO_2 electrolyzers. Joule *8*, 1754–1771. https://doi.org/10.1016/j.joule.2024.02.027.
25. Milosevic, M., Böhm, T., Körner, A., Bierling, M., Winkelmann, L., Ehelebe, K., Hutzler, A., Suermann, M., Thiele, S., and Cherevko, S. (2023). In Search of Lost Iridium: Quantification of Anode Catalyst Layer Dissolution in Proton Exchange Membrane Water Electrolyzers. ACS Energy Lett. *8*, 2682–2688. https://doi.org/10.1021/acsenergylett.3c00193.
26. Dam, A.P., Abuthaher, B.Y.A., Papakonstantinou, G., and Sundmacher, K. (2023). Insights into the Path-Dependent Charge of Iridium Dissolution Products and Stability of Electrocatalytic Water Splitting. J. Electrochem. Soc. *170*, 064504. https://doi.org/10.1149/1945-7111/acd4f2.
27. Hartig-Weiss, A., Tovini, M.F., Gasteiger, H.A., and El-Sayed, H.A. (2020). OER Catalyst Durability Tests Using the Rotating Disk Electrode Technique: The Reason Why This Leads to Erroneous Conclusions. ACS Appl. Energ. Mater. *3*, 10323–10327. https://doi.org/10.1021/acsaem.0c01944.
28. Zlatar, M., Escalera-López, D., Rodríguez, M.G., Hrbek, T., Götz, C., Mary Joy, R.M., Savan, A., Tran, H.P., Nong, H.N., Pobedinskas, P., et al. (2023). Standardizing OER Electrocatalyst Benchmarking in Aqueous Electrolytes: Comprehensive Guidelines for Accelerated Stress Tests and Backing Electrodes. ACS Catal. *13*, 15375–15392. https://doi.org/10.1021/acscatal.3c03880.
29. Alia, S.M., Ha, M.A., Anderson, G.C., Ngo, C., Pylypenko, S., and Larsen, R.E. (2019). The Roles of Oxide Growth and Sub-Surface Facets in Oxygen Evolution Activity of Iridium and Its Impact on Electrolysis. J. Electrochem. Soc. *166*, F1243–F1252. https://doi.org/10.1149/2.0771915jes.
30. De Luna, P., Quintero-Bermudez, R., Dinh, C.T., Ross, M.B., Bushuyev, O.S., Todorović, P., Regier, T., Kelley, S.O., Yang, P.D., and Sargent, E.H. (2018). Catalyst electro-redeposition controls morphology and oxidation state for selective carbon dioxide reduction. Nat. Catal. *1*, 103–110. https://doi.org/10.1038/s41929-017-0018-9.
31. Zhang, J.X., Litteer, B.A., Gu, W., Liu, H., and Gasteiger, H.A. (2007). Effect of hydrogen and oxygen partial pressure on pt precipitation within the membrane of PEMFCs. J. Electrochem. Soc. *154*, B1006. https://doi.org/10.1149/1.2764240.

32. Dominguez, D.C., Dam, A.P., Alia, S.M., Richter, T., and Sundmacher, K. (2025). Application of a temporal multiscale method for efficient simulation of degradation in PEM Water Electrolysis under dynamic operating conditions. Comput. Chem. Eng. *198*, 109083. https://doi.org/10.1016/j.compchemeng.2025.109083.

33. Franz, T., Papakonstantinou, G., and Sundmacher, K. (2023). Transient hydrogen crossover in dynamically operated PEM water electrolysis cells- A model-based analysis. J. Power Sources *559*, 232582. https://doi.org/10.1016/j.jpowsour.2022.232582.

34. Trinke, P., Bensmann, B., Reichstein, S., Hanke-Rauschenbach, R., and Sundmacher, K. (2016). Hydrogen Permeation in PEM Electrolyzer Cells Operated at Asymmetric Pressure Conditions. J. Electrochem. Soc. *163*, F3164–F3170. https://doi.org/10.1149/2.0221611jes.

35. Dam, A.P., Franz, T., Papakonstantinou, G., and Sundmacher, K. (2025). Catalyst dissolution in PEM water electrolysis: Influence of time, current density and Iridium ion transport in single-pass and recirculation water flow modes. Appl. Catal. B *365*, 124946. https://doi.org/10.1016/j.apcatb.2024.124946.